

Effect of IGF-1C domain-modified nanoparticles on renal ischemia–reperfusion injury in mice

Meng Xu, Mingyue Zhao and Donghui Zheng

Department of Nephrology, Affiliated Huai'an Hospital of Xuzhou Medical University, Huai'an, China

ABSTRACT

Renal ischemia–reperfusion injury (IRI) is a common prerequisite of acute renal injury (AKI) that involves the entire system and induces critical illness. The C domain of insulin-like growth factor-1 (IGF-1C) plays an important role in promoting angiogenesis and enhancing the inflammatory response. However, given the shortcomings of its short half-life and poor stability, the application of IGF-1C is restricted. In the present study, IGF-1C nanoparticles (NP-IGF-1C) were constructed by combining 1,2-distearoyl-sn-glycero-3-phosphoethanolamine-N-[maleimide (polyethylene glycol)](DSPE-PEG-MAL) and IGF-1C through a Michael addition reaction to evaluate the effects of NP-IGF-1C on preventing IRI. *In vitro* studies have shown that NP-IGF-1C is not cytotoxic and protects cells from oxidative damage. The renal enrichment and biocompatibility of NP-IGF-1C were determined *in vivo* by connecting fluorescent molecules to NP-IGF-1C for *in vivo* imaging and pathological staining of important organs. After IRI, renal function decreased, and inflammatory cell infiltration, oxidative stress and apoptosis increased. As expected, NP-IGF-1C reversed these changes, indicating that NP-IGF-1C played a protective role in the process of IRI, which may be mediated by its antioxidant, anti-inflammatory and antiapoptotic activities.

ARTICLE HISTORY

Received 14 February 2022
Revised 14 June 2022
Accepted 1 July 2022

KEYWORDS

Renal ischemia–reperfusion;
C domain of insulin-like
growth factor; NP-IGF-1C;
acute kidney injury;
antioxidant

Introduction

As a common clinical syndrome, acute kidney injury (AKI) is characterized by a rapid decline in renal function and a decrease in the glomerular filtration rate, with the clinical manifestations of oliguria, anuria, edema, anorexia, and chest tightness. AKI occurs with the rapid decline in renal function in a short time caused by various factors and is usually critical [1]. According to statistics, approximately 10–15% of hospitalized patients experience AKI, and 5% of hospitalized patients require lifelong dialysis, making prevention and treatment urgent needs [2,3]. Early diagnosis and treatment contribute to improving the patient prognosis.

Accounting for 60% of AKI etiologies, renal ischemia reperfusion injury (IRI) refers to the process of an initial restriction of the blood supply to kidney and subsequent reperfusion of the tissue with blood. The prevalence of ischemic AKI is increasing worldwide, especially in critically ill patients or patients undergoing major surgery [4,5]. However, no effective therapeutic interventions are available to prevent, reduce or repair

acute tubular necrosis (ATN) in clinical practice. Therefore, drugs with potential therapeutic value must be identified.

Insulin-like growth factor-1 (IGF-1) is essential for normal growth and development. Furthermore, IGF-1 is important for the normal development of prenatal and postpartum kidneys and is considered to play an important role in facilitating the recovery of renal function in individuals with AKI [6,7]. IGF-1 is a long-chain polypeptide composed of dozens of amino acids, including four domains, A, B, C and D. The C domain peptide (IGF-1C) is considered the active domain of IGF-1.

However, the circulating half-life of peptides is considerably less than that required for frequent use. The absorption, distribution, metabolism and excretion of peptides can be improved by increasing cell permeability, enhancing chemical and proteolytic stability and reducing the overall clearance in the kidney to prolong the cycling half-life.

Nanotechnology has emerged as a tool to solve these problems. Drugs consisting of peptides

incorporated in nanoparticles have the potential to reduce the side effects and toxicity associated with the current available treatments for renal diseases and may produce higher intrarenal drug concentrations than free drugs. Given its beneficial features, such as biocompatibility, nontoxicity, inexpensiveness and nonimmunogenicity, polyethylene glycol (PEG) is an ideal candidate material for modification [8]. Furthermore, the ability of PEG to increase binding with plasma proteins, including albumin, and decrease renal clearance has been extensively explored. In 2018, Wang *et al.* developed a PEG-based dexamethasone macromolecular prodrug (ZSJ-0228) that self-assembles into micelles in aqueous medium, penetrates into inflammatory sites through leaky blood vessels, and locally releases active drugs. Compared with daily treatment with the same dose of dexamethasone 21-phosphate, monthly intravenous injection of ZSJ-0228 for two months significantly increased the survival rate of lupus-susceptible NZB/WF1 mice and alleviated proteinuria with no obvious systemic toxicity [9].

In the present study, DSPE-PEG-MAL was connected to IGF-1C through a Michael addition reaction to construct nanoparticles (NP-IGF-1C). We evaluated whether NP-IGF-1C improved the renal function of the mouse IRI model and explored its mechanism of alleviating renal injury to provide a new theoretical basis and scientific guidance for the treatment of AKI.

Materials and methods

Animals and groups

Twenty male BALB/c mice (20–30 g, 8 weeks) supplied by the Laboratory Animal Center of Nankai University were used in the current study. Mice were fed a standard mouse chow diet throughout the study and were housed (five per cage) under controlled laboratory conditions (12/12: light/dark, $23 \pm 2^\circ\text{C}$, $60 \pm 10\%$ humidity). All animal studies were performed according to the guidelines established by the Tianjin Committee of Use and Care of Laboratory Animals, and the overall project protocols were approved by the Animal Ethics Committee of Nankai University. The accreditation number of the laboratory is SYXK (Jin) 2019–0003 promulgated by Tianjin Science and Technology Commission. Mice were randomized into four groups: sham, sham operation group (abdominal surgical exploration + tail vein injection of PBS); IRI, IRI model group (renal ischemia–reperfusion surgery + tail vein injection of PBS); IGF-1C + IRI, IGF-1C treatment group (renal ischemia–reperfusion surgery + tail vein injection of IGF-1C); and NP-IGF-1C + IRI, NP-IGF-1C treatment group (renal

ischemia–reperfusion surgery + tail vein injection of NP-IGF-1C). Mice were injected with 200 μL of PBS, IGF-1C or NP-IGF-1C 2 h before the operation and 24 h and 48 h after the operation. The IGF-1C solution was obtained by dissolving 25 mg of the IGF-1C polypeptide in 1 mL of PBS.

Synthesis and characterization of NP-IGF-1C and NP

First, 1 mL of tetrahydrofuran was added to dissolve the mixture of fluorescent molecules TPE-PH-DCM (1 mg, synthesized in our laboratory) and DSPE-PEG-MAL₅₀₀₀ (3 mg, purity $\geq 99\%$, Tianjin Haoyang Biological Products Co., Ltd. Tianjin, China). Second, this solution was slowly added to ultrapure water (9 mL) and sonicated with an ultrasonic cell crusher for 3 min, followed by volatilization to remove tetrahydrofuran. Next, the remaining solution was ultrafiltered to 1 mL to obtain 1 mg/mL nanoparticles, and the nanoparticles were dialyzed in ultrapure water thrice to completely remove tetrahydrofuran. Finally, IGF-1C (2.5 mg, purity $\geq 98\%$, Jili Biochemical Co., Ltd.) was added to the aforementioned solution, and the mixture was placed on a shaking table overnight to allow the nanoparticles to completely bind polypeptides and obtain NP-IGF-1C nanoparticles.

Only DSPE-PEG-MAL5000 was added to ultrapure water and sonicated with an ultrasonic cell crusher, followed by volatilization to remove tetrahydrofuran and ultrafiltration to obtain 1 mg/mL blank nanoparticles (NPs). The specific procedures were the same as those used for the synthesis of NP-IGF-1C.

After obtaining the nanoparticle solution, the sample cells containing the NP solution and IGF-1C solution were individually placed into a Zetasizer Nano ZS (Malvern Instruments, UK) to measure the size and potential. They were also dropped on a copper mesh to assess the ultrastructure with transmission electron microscopy (TEM).

Determination of the encapsulation efficiency and drug loading

First, the UV absorption of polypeptide molecules with different masses was measured to generate the standard curve. By measuring the UV absorption of NP-IGF-1C, which was substituted into the standard curve, the mass of the remaining polypeptide molecules in the solution was calculated. The drug loading (DL%) and encapsulation efficiency (EE%) were calculated using the following formulas: $\text{DL}\% = \frac{\text{drug weight in}}$

nanoparticles/(carrier mass + drug mass in nanoparticles) × 100%; EE% = weight of drug in nanoparticles/weight of drug initially added × 100%, DL% = drug weight in nanoparticles/(carrier mass + drug mass in nanoparticles) × 100%.

MTT assay

Cell viability was measured using the 3-(4,5-dimethyl-2-thiazolyl)-2,5-diphenyl-2-H-tetrazolium bromide (MTT) assay. A total of 5×10^3 human embryonic kidney cells (HEK293 cells) were seeded in each well of 96-well plates, which were divided in accordance with experimental experience and the related literature into 6 groups (control, H₂O₂ (100 μM), H₂O₂ (100 μM)+NP-IGF-1C, H₂O₂ (100 μM)+IGF-1C, H₂O₂ (100 μM)+NP, and NP-IGF-1C). After 24 h of treatment, the cultured cells were incubated with an MTT solution (0.5 mg/mL) for 2 h, and the optical density (OD) values at 570 nm were obtained.

Live-dead staining of cells

HEK293 cells were incubated in confocal microscopy dishes at a density of 5×10^4 cells/dish at 37 °C in a 5% carbon dioxide incubator for 24 h. After the incubation, the cells were incubated with PBS, H₂O₂ (100 μM), H₂O₂ (100 μM)+NP-IGF-1C, H₂O₂ (100 μM)+IGF-1C, H₂O₂ (100 μM)+NP or NP-IGF-1 for an additional 24 h. Next, the Calcein/PI Cell Viability/Cytotoxicity Assay Kit (Beyotime, Cat: C2015 M, Shanghai, China) was used to detect living and dead cells according to the manufacturer's instructions. Finally, the cells were viewed under a fluorescence microscope, and cell viability was calculated using the following equation: cell viability (%) = (number of calcein-AM + cells)/(number of calcein-AM + cells + number of PI + cells) × 100.

Construction of the renal ischemia–reperfusion injury model

Mice were anesthetized with isoflurane throughout the procedure. The skin was incised along the midline of the back of each mouse, and both kidneys were exposed. After separating and clamping both renal arteries for 45 min to block blood flow to the kidney, the color of the kidney changed from red to dark purple, indicating renal ischemia. The artery clamps were removed 45 min later. The color of the kidneys gradually returned to bright red, and the back incision was sutured.

Imaging of main organs and fluorescence decays of NP-IGF-1C in kidneys

Two mice each from the sham operation group and operation group were randomly selected and injected with 200 μL of the NP-IGF-1C solution through the caudal vein. Under the conditions of an excitation wavelength of 465 nm and an emission wavelength of 640 nm, the relevant parameters were adjusted to collect images. The kidneys of mice in the operation group were collected images at 3, 6, 9 and 12 hours respectively. Data were analyzed using Living Image software.

Blood and tissue sample collection

Seventy-two hours after the reperfusion phase, mice were anesthetized with isoflurane, and blood samples were collected by removing the left eyeball of the mice. The blood samples were incubated at room temperature for 2 h and then centrifuged at 3000 rpm for 5 min to obtain serum samples, which were separated and stored at –80 °C. The heart, liver, spleen, liver and one kidney were collected from each mouse and placed in a 10% formalin solution for histological assessment, whereas the other kidney was preserved at –80 °C for additional measurements.

Evaluation of biomarkers of renal injury

Using a biochemical automatic analyzer, the stored serum samples were used to measure the levels of serum creatinine (Scr) and blood urea nitrogen (BUN), which are markers of prevailing renal function and are used for AKI diagnoses. Serum levels of Kidney Injury Molecule-1 (KIM-1) and NAGL were measured using ELISA kits according to the manufacturer's protocols.

Determination of oxidative stress

Tissue lysis buffer was added to kidney tissue samples of the same weight and ground with a glass homogenizer (1 mL) on ice, followed by centrifugation at 1500 × g for 30 min at 4 °C to collect the supernatant containing proteins. Before the determination of lipid peroxidation indicators, the protein concentration was calculated with the BCA protein assay, and the concentrations of lysates were adjusted accordingly. Renal activities of catalase (CAT), malondialdehyde (MDA), and glutathione peroxidase (GSH-Px) were determined using a CAT determination kit, MDA determination kit and GSH determination kit (Beyotime, Shanghai, CN), respectively, with a multifunctional microplate reader.

Western blotting

After the kidney tissue samples were lysed in RIPA buffer containing 1 mM PMSF, protein concentrations were detected using a BCA kit. The samples were electrophoresed on 10% SDS-PAGE gels and transferred to PVDF membranes. Next, the membranes were blocked with rapid blocking solution, incubated with primary antibodies overnight, and then incubated with secondary antibodies. The membranes were observed using chemiluminescence imaging (Clinx Science Instruments Co., Ltd.). Protein bands were quantified by densitometry using ChemiAnalysis software (Clinx Science Instruments Co., Ltd.).

Immunofluorescence staining

The kidneys were placed into a gradient of sucrose solutions for dehydration and then placed in the embedding solution. Next, the dehydrated and embedded kidneys were cut into 5- μ m-thick frozen sections using a cryostat microtome (LEICA, GER). Then, the samples were fixed and blocked with acetone, Triton-X100, H₂O₂ and goat serum. After an incubation with primary antibody overnight and an incubation with secondary antibody for 1 h, the samples were incubated with DAPI. Finally, a field of view was randomly selected and photographed with a confocal microscope (LSM 800 with Airyscan, GER).

Histopathological evaluation

The kidney, heart, liver, spleen and lung tissues were fixed with 4% paraformaldehyde for 48 h and then rinsed repeatedly with PBS to remove the residual fixative solution. Next, the tissues were sequentially placed in embedding cassettes and in an automatic dehydrator until the samples were dehydrated, dipped in ethanol and xylene, and embedded in paraffin.

After the tissue samples were removed, they were cut into 5- μ m-thick sections and stained with an HE staining kit (Solarbio, Beijing, China) according to the manufacturer's instructions. HE-stained sections were randomly selected from each group for observation and photographed using a light microscope (DM2500, Leica, Wetzlar, Germany). High-power fields of view were randomly selected during imaging to ensure a fair comparison.

TUNEL assay

The terminal deoxynucleotidyl transferase dUTP nick end labeling (TUNEL) assay was conducted using an

apoptosis detection kit (KGA702, Nanjing, China) according to the manufacturer's protocol to determine the percentage of apoptotic cells. TUNEL-positive cells were counted at 100 \times magnification in the cross-sections by a researcher who was blinded to the protocol. All measurements were performed in a blinded manner.

Evaluation of inflammatory factors in serum

Levels of inflammatory factors (IL-6 and IL-10) were determined using enzyme-linked immunosorbent assay (ELISA) with an IL-6 ELISA kit and an IL-10 ELISA kit purchased from Abclonal (Wuhan, CN), respectively. The samples analyzed were serum, and the tests were performed according to the instructions. Finally, a multi-functional microplate reader was used to measure the absorbance of the samples at 450 nm.

Statistical analysis

Statistical analyses were performed using SPSS 22.0 statistical software (IBM, USA). All measurement data are presented as the means \pm standard deviations ($M \pm SD$), and comparisons between two groups were conducted with an independent sample test.

Results

Characterization of NP-IGF-1C and NPs

Under the transmission electron microscope, the morphology of NP-IGF-1C and NPs was approximately spherical (Figure 1(A)). Dissolved NP-IGF-1C was observed as a transparent yellow liquid (Figure 2(A)). Due to the slight negative charges, the sizes of the NP-IGF-1C and NPs in this study were 94.87 nm (PDI = 0.174) and 59.58 nm (PDI = 0.169), respectively (Figure 1(B,C)). The excitation wavelength of TPE-Ph-DCM, a fluorescent dye carried by NP-IGF-1C, was 465 nm, and the emission wavelength was 640 nm. Imaging under these conditions revealed minimal fluorescence aggregation in the kidneys of sham mice, whereas a large amount of fluorescence accumulated in the kidneys of mice with IRI. Otherwise, the other main organs of the two groups of mice showed no obvious fluorescence (Figure 2(B)). The attenuation of fluorescence signal takes 12 hours, indicating that NP-IGF-1C can stay in the kidney for a long time (Figure 2(C)).

Cytoprotective effects of NP-IGF-1C

H₂O₂ is a strong oxidizing reagent, and even if a minimal concentration of H₂O₂ is added to the cells, it will

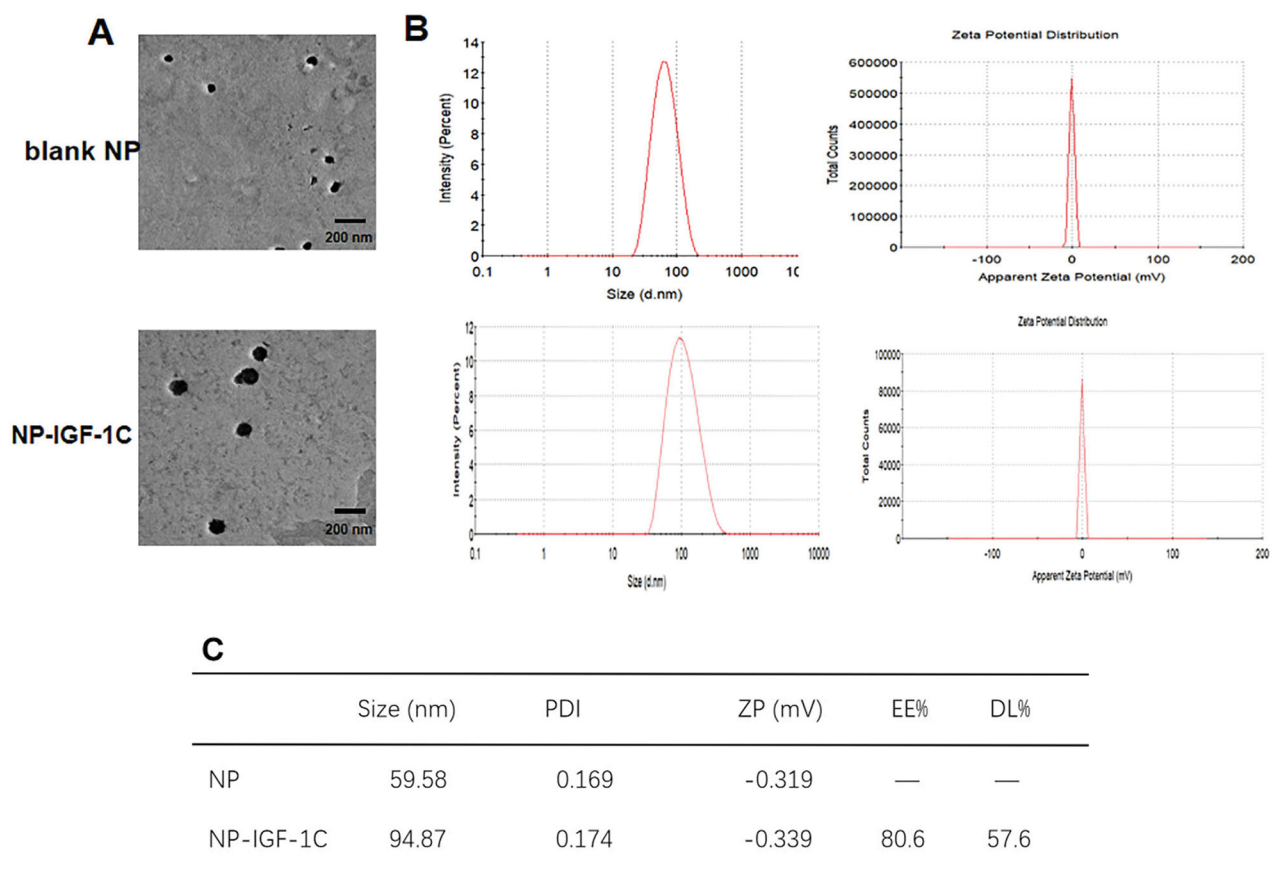


Figure 1. Characterization of NP-IGF-1C. (A) Transmission electron microscopy (TEM) images of NP-IGF-1C and NPs. Scale bar = 200 nm. (B, C) Size, zeta potential, PDI, EE% and DL% of NP-IGF-1C and NPs.

cause intracellular oxidative stress and cell death. After H_2O_2 was incubated with HEK 293 cells for 24 h, the relative survival rate of HEK 293 cells was measured using the MTT method. Clearly, the survival rate of cells decreased significantly. However, through the protective effects of IGF-1C and NP-IGF-1C, the cell survival rate increased, indicating that IGF-1C and NP-IGF-1C prevented H_2O_2 -mediated damage to HEK293 cells. Among these two treatment, NP-IGF-1C exerted the greatest protective effect. The low OD of the H_2O_2 + NP group indicated that the cytoprotective effect of NP-IGF-1C was not dependent on NPs. In addition, we also observed the nontoxicity of NP-IGF-1C based on the high OD of the NP-IGF-1C group (Figure 3(C)).

Live-dead staining of HEK293 cells was conducted to detect the antioxidant activity of NP-IGF-1C. The survival rate of cells treated with NP-IGF-1C was similar to that of the control group, indicating the good biocompatibility of NP-IGF-1C. A large number of cells died in the H_2O_2 group due to oxidative damage, whereas the cell survival rates in the H_2O_2 + IGF-1C group and H_2O_2 + NP-IGF-1C group were significantly greater than

those in the H_2O_2 group, revealing the capacities of IGF-1C and NP-IGF-1C to protect cells from oxidative damage. A greater number of live cells was observed in the H_2O_2 + NP-IGF-1C group than the H_2O_2 + IGF-1C group, and the number of live cells in the H_2O_2 + NP group was similar to that in the H_2O_2 group (Figure 3(A,B)).

Analysis of biomarkers of renal injury

As shown in Figure 4(A), higher Scr and BUN levels, which indicate renal failure, were noted in IRI mice. However, the levels of these two indicators decreased after IGF-1C injection. In addition, their levels were significantly decreased after the injection of NP-IGF-1C, indicating that NP-IGF-1C treatment reduced renal damage in IRI mice. Figure 4(B) shows that IRI significantly upregulated renal KIM-1 and neutrophil gelatinase-associated lipocalin (NGAL) expression compared to the sham treatment. Compared with sham rats, NP-IGF-1C and IGF-1C treatment significantly reduced KIM-1 and NGAL expression in renal tissue. Furthermore, the

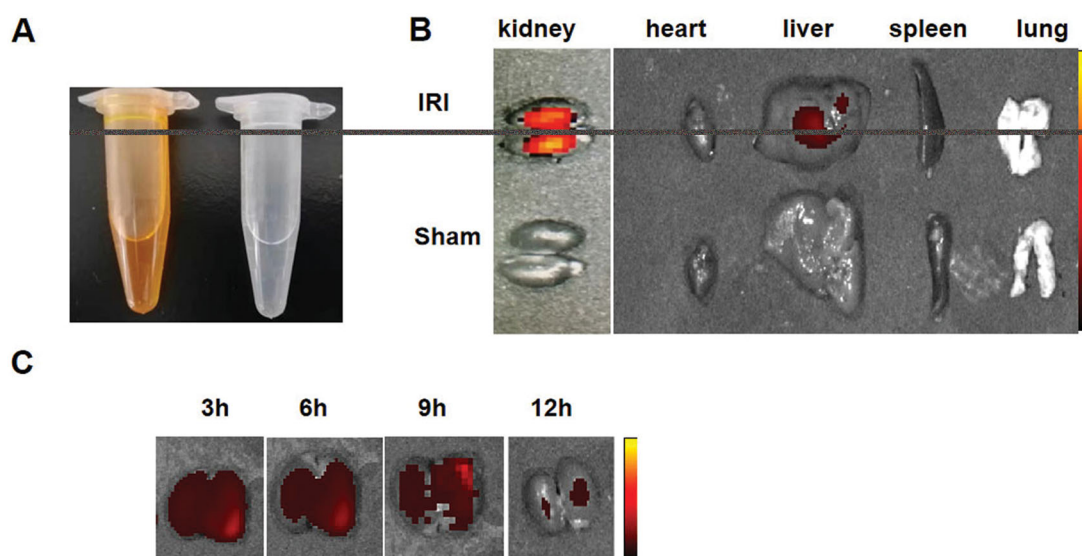


Figure 2. (A) NP-IGF-1C nanoparticle solution (left panel) and IGF-1C solution (right panel). (B) Fluorescence signal of NP-IGF-1C in the main organs. (C) Fluorescence signal of NP-IGF-1C was attenuated in the kidney. The quantities indicated by the color bar ranged from 320 to 500 cps.

administration of NP-IGF-1C downregulated KIM-1 and NGAL expression compared to IGF-1C administration.

Figure 4(B) shows that IRI significantly upregulated renal KIM-1 and neutrophil gelatinase-associated lipocalin (NGAL) expression compared to the sham treatment. Compared with sham rats, NP-IGF-1C and IGF-1C treatment significantly reduced KIM-1 and NGAL expression in renal tissue. Furthermore, the administration of NP-IGF-1C downregulated KIM-1 and NGAL expression compared to IGF-1C administration.

NP-IGF-1C pretreatment altered antioxidant enzyme levels in the renal IRI model

Figure 5 shows the relative activities of the 3 different antioxidant enzymes. GSH-Px and CAT levels in the IRI group were significantly lower than those in the sham group. Compared with the IRI group, the IGF-1C group displayed increased GSH-Px and CAT levels. However, the NP-IGF-1C group exhibited more obvious increases in the activities of these enzymes (Figure 5(A,B)). Tissue MDA levels are shown in Figure 5(C). MDA levels in the IRI group were significantly increased compared with those in the sham group ($p < .001$), whereas MDA levels in the IGF-1C group were decreased. Furthermore, the decrease was more pronounced in the NP-IGF-1C group.

NP-IGF-1C decreased apoptosis

Immunofluorescence staining for Bax (Figure 6(A)) and western blot analyses of Bcl-2 and Bax levels (Figure 6(B,C)) were performed to further investigate the

mechanism by which NP-IGF-1C attenuates renal cell apoptosis after IRI. Although Bcl-2 levels in the IGF-1C group were higher than those in the IRI group, the highest Bcl-2 levels were detected in the NP-IGF-1C group. In contrast, Bax protein levels in the NP-IGF-1C group were lower than those in the IGF-1C group and even lower than those in the IRI group.

In addition, the number of TUNEL-positive cells was increased significantly in the IRI group, whereas the numbers of TUNEL-positive cells were decreased in the NP-IGF-1C group and IGF-1C group. The lower number of TUNEL-positive cells indicated the superior antiapoptotic activities of NP-IGF-1C (Figure 7(A,B)). Therefore, NP-IGF-1C directly and rapidly protected the kidneys of IRI mice.

NP-IGF-1C decreased pathological injury

As illustrated in Figure 7(C), the kidney tissue structures of the sham group exhibited no notable histopathological features under a microscope (HE staining). In contrast, severe renal tubular injury and pathological changes occurred in mice in the IRI group. The degree of acute tubular necrosis was evaluated by counting indices, such as renal tubular expansion and abscission, protein tubular type, brush border loss and cellular necrosis [10]. The IGF-1C treatment reduced the degree of renal tubular injury after surgery, suggesting that IGF-1C alleviated renal injury caused by ischemia and promoted tissue repair. In addition, the tissue of the NP-IGF-1C group exhibited less injury than that of the IGF-1C group, indicating that NP-IGF-1C more effectively reduced renal pathological damage caused by IRI (Figure 7(D)).

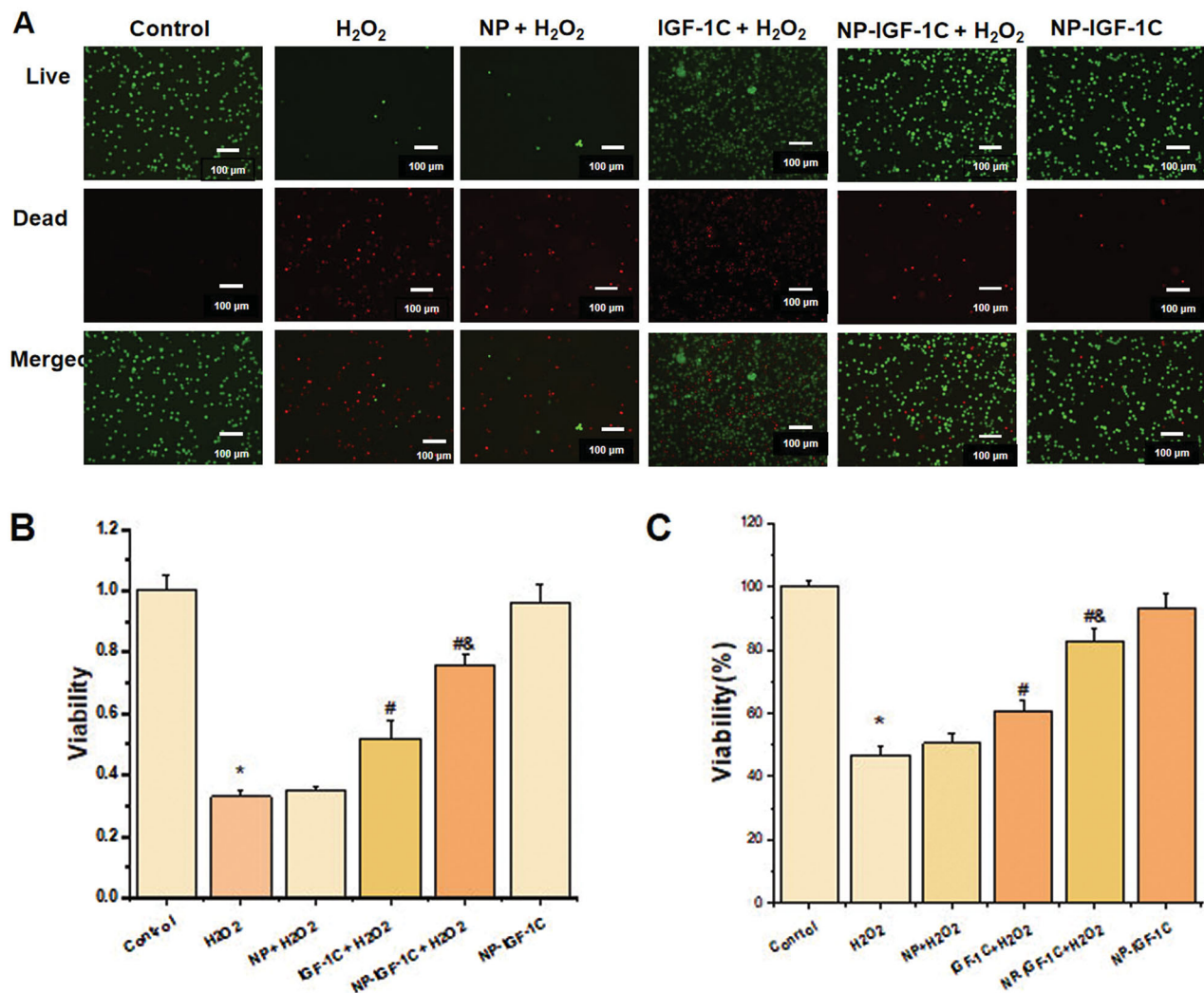


Figure 3. Cytoprotective effects of NP-IGF-1C. (A, B) Live-dead staining and quantification of cell viability (%) in each group. Scale bar = 100 μ m. (C) MTT assay showing the optical density (OD) values of HEK293 cells incubated with various treatments for 24 h. Error bars represent the $M \pm SD$ from three independent experiments. * $p < 0.05$ compared with the control group; # $p < 0.05$ compared with the H₂O₂ group. IGF-1C, C domain of insulin-like growth factor-1; NP-IGF-1C, nanoparticles of NP-IGF-1C.

NP-IGF-1C inhibited inflammatory cytokine production

As shown in Figure 8, serum IL-6 concentrations in the IRI group were significantly increased compared with those in the sham group, and IGF-1C treatment reduced IL-6 production. In addition, IL-6 levels were further reduced in the NP-IGF-1C group. IL-10 levels in the blood of mice in the IRI group decreased, whereas IGF-1C treatment increased IL-10 levels. This increase in IL-10 levels was more obvious in the NP-IGF-1C group, suggesting that NP-IGF-1C exerted a protective effect by reducing the inflammatory response in kidneys suffering ischemia–reperfusion.

In vivo evaluation of NP-IGF-1C toxicity

NP-IGF-1C (200 μ L/day) was injected intravenously into normal mice to evaluate its biosafety. After 3 days, the

major organs, including the heart, liver, lungs and spleen, were collected from the mice. Compared with the control group, the main organs of normal mice were not significantly damaged (Figure 9), indicating that NP-IGF-1C did not induce adverse side effects on healthy mice and exhibited excellent biocompatibility *in vivo*.

Discussion

This experiment using the IVIS Spectrum small animal *in vivo* imaging system revealed that NP-IGF-1C administered through the caudal vein was enriched in the kidneys of mice suffering from ischemia–reperfusion injury induced by clamping the bilateral renal arteries. IRI, which caused by an abrupt cessation of blood flow into a specific organ, can occur after heart failure, severe trauma and surgery and aggravate tissue damage by

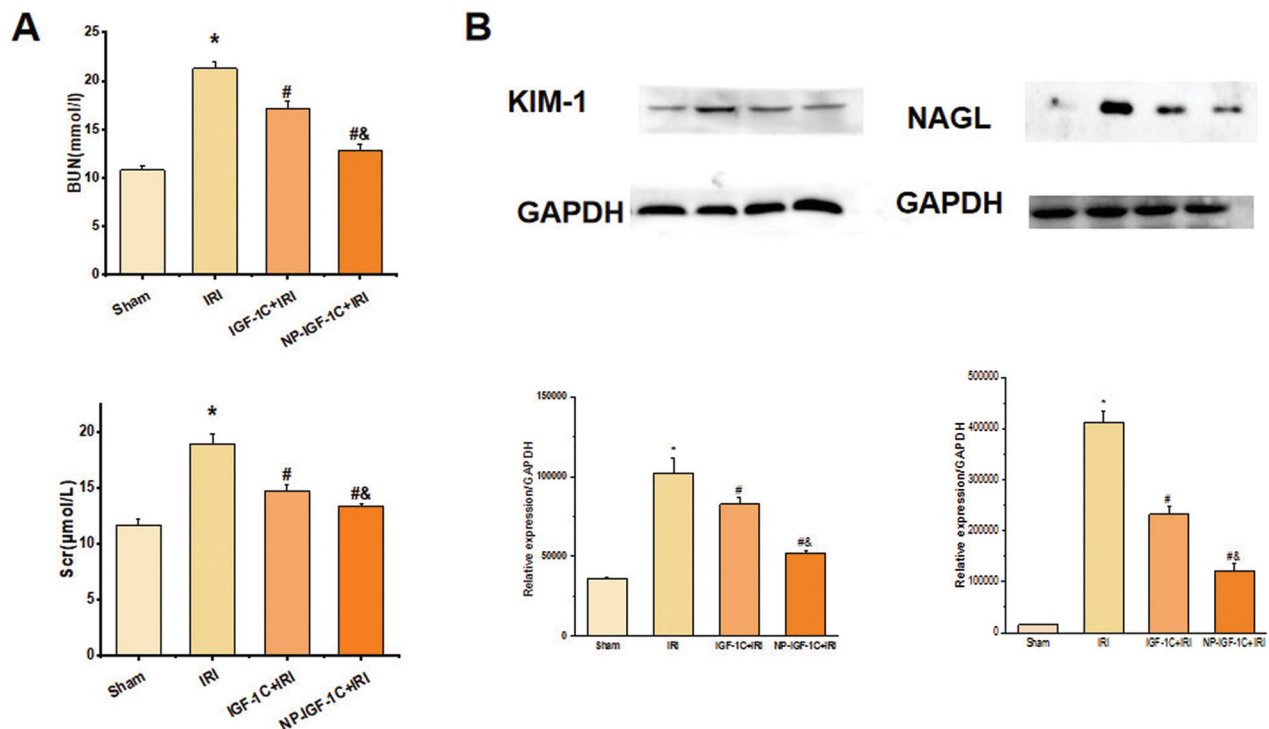


Figure 4. SCr, BUN, KIM-1 and NAGL levels, which are biomarkers of renal injury, were detected at Day 3 postinjury. Data are presented as $M \pm SD$; $n = 5$. * $p < 0.05$ compared with the sham group; # $p < 0.05$ compared with the IRI group; & $p < 0.05$ compared with the IRI+IGF-1C group. SCr, serum creatinine; BUN, blood urea nitrogen; KIM-1, Kidney Injury Molecule-1; NAGL, neutrophil gelatinase-associated lipocalin; IRI, ischemia–reperfusion injury; IGF-1C, C domain of insulin-like growth factor-1; NP-IGF-1C, nanoparticles of NP-IGF-1C.

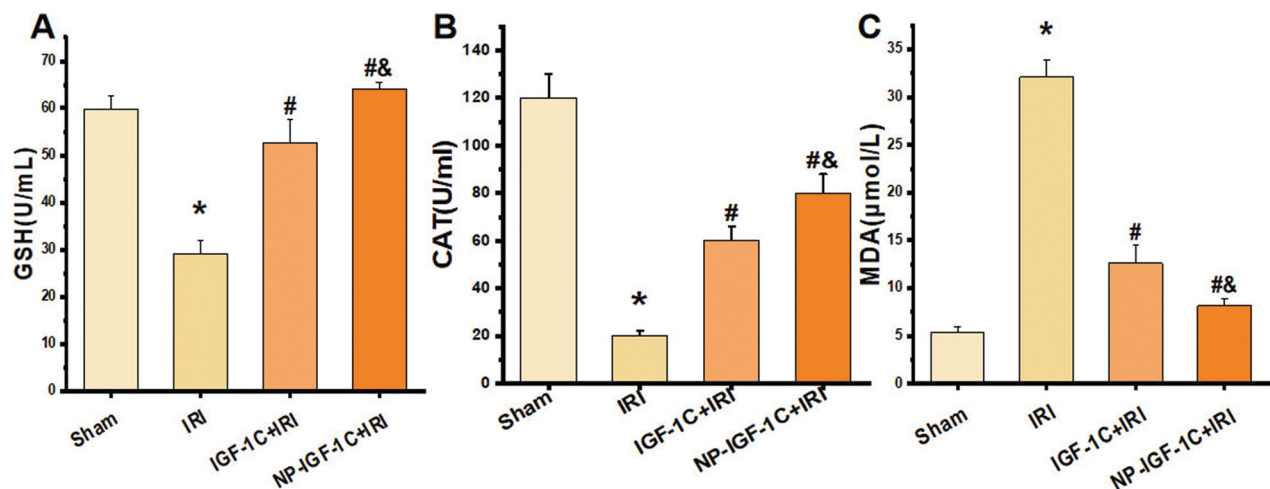


Figure 5. GSH-Px, CAT and MDA levels were detected at Day 3 postinjury. Data are presented as $M \pm SD$; $n = 5$. * $p < 0.05$ compared with the sham group; # $p < 0.05$ compared with the IRI group; & $p < 0.05$ compared with the IRI+IGF-1C group. IRI, ischemia–reperfusion injury; IGF-1C, C domain of insulin-like growth factor-1; NP-IGF-1C, nanoparticles of NP-IGF-1C; GSH-Px, glutathione peroxidase; CAT, catalase; MDA, malondialdehyde.

initiating oxidative stress, the inflammatory response and apoptosis pathways [11,12].

When IRI is initiated, it causes a series of pathological injuries to renal tissue, including tubular epithelial necrosis, degeneration and abscission, lumen expansion, interstitial congestion and inflammatory cell

infiltration [13]. *In vivo* experiments showed that treatment with NP-IGF-1C reduced Scr, BUN and tubular injury scores compared to PBS.

As a significant feature of early acute kidney injury, inflammatory cell infiltration occurs within 2 h after ischemic injury [14]. As a major proinflammatory

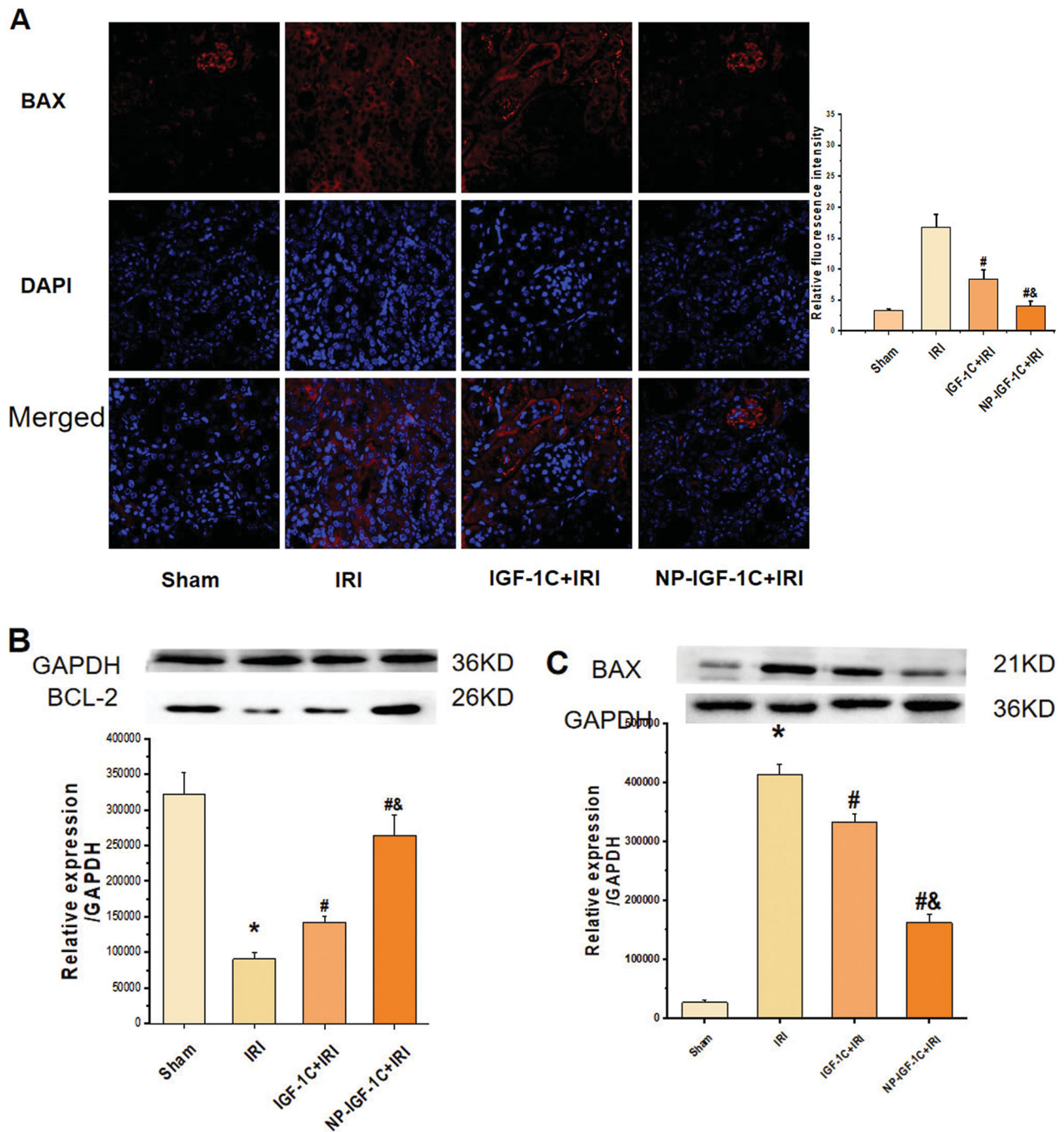


Figure 6. (A) Bax expression in renal tissues was analyzed using immunofluorescence staining. Scale bar = 50 μ m. (B, C) Bax and Bcl-2 protein levels in renal tissues were quantified using western blotting. Error bars represent the $M \pm SD$ from three independent experiments. * $p < 0.05$ compared with the sham group; # $p < 0.05$ compared with the IRI group; & $p < 0.05$ compared with the IRI+IGF-1C group. IRI, ischemia–reperfusion injury; IGF-1C, C domain of insulin-like growth factor-1; NP-IGF-1C, nanoparticles of NP-IGF-1C.

mediator, IL-6 levels increased earlier than the levels of other cytokines (such as the systemic inflammatory marker C-reactive protein) during the inflammatory response. On the other hand, IL-10 is a potent immunomodulator with anti-inflammatory and tissue regenerative activities [15] that antagonizes the effect of IL-6. Studies have revealed that IL-10 prevents renal injury caused by ischemia, cisplatin nephrotoxicity or ureteral obstruction

by limiting the infiltration of immune cells and the production of inflammatory cytokines [15]. Because IRI triggers the inflammatory cascade, it results in greater renal damage, and inhibition of the inflammatory response is a therapeutic method to protect renal tissue. Treatment with NP-IGF-1C decreased IL-6 levels and increased IL-10 levels, confirming its ability to reduce the inflammatory response after renal tubular injury.

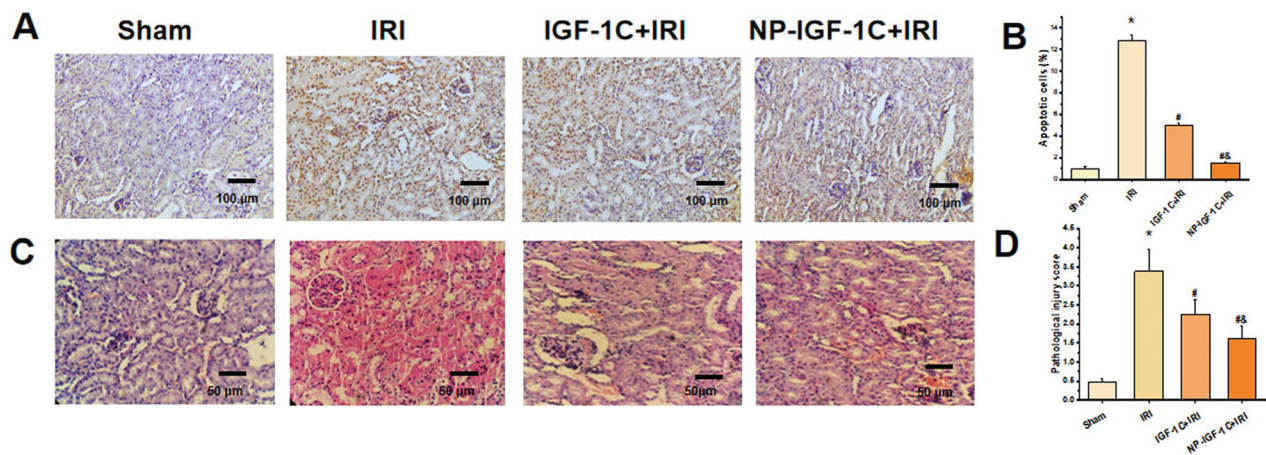


Figure 7. (A) TUNEL-positive apoptotic kidney cells and TUNEL-negative (nonapoptotic, normal) kidney cells. (B) The percentage of TUNEL-positive apoptotic kidney cells. (C) Hematoxylin and eosin (HE) staining of kidney tissues from each group. Scale bar = 50 μm . (D) Semiquantitative histological assessment of HE staining by determining the acute tubular necrosis (ATN) score. * $p < 0.05$ compared with the sham group; # $p < 0.05$ compared with the IRI group; & $p < 0.05$ compared with the IRI+IGF-1C group. Error bars represent the $M \pm SD$ from three independent experiments. IRI, ischemia–reperfusion injury; IGF-1C, C domain of insulin-like growth factor-1; NP-IGF-1C, nanoparticles of NP-IGF-1C.

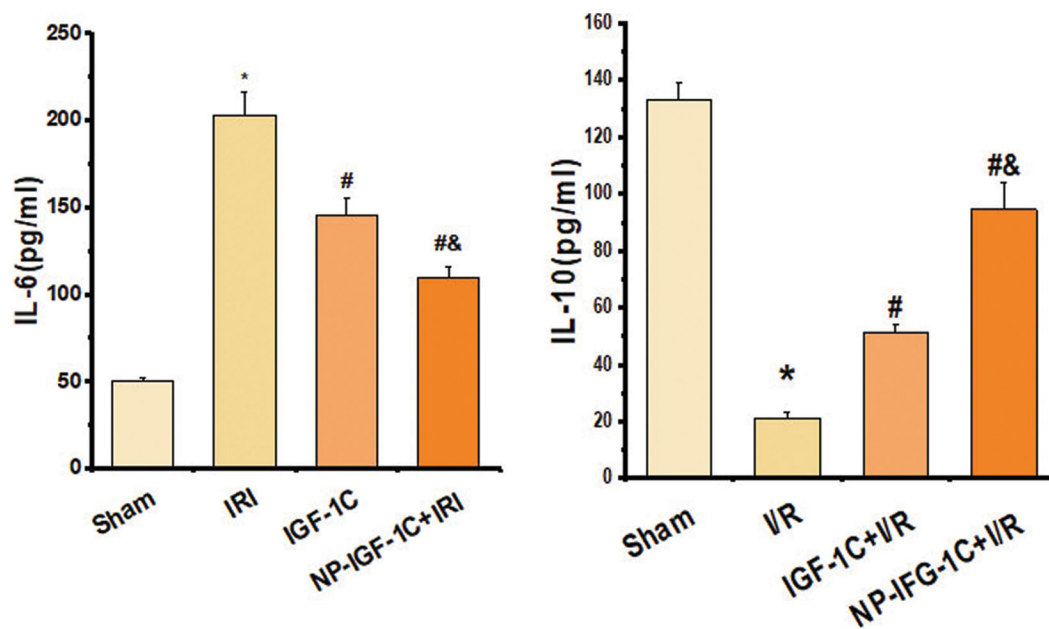


Figure 8. Inflammatory cytokine (IL-6 and IL-10) levels were detected at Day 3 postinjury ($n = 5$). * $p < 0.05$ compared with the sham group; # $p < 0.05$ compared with the IRI group; & $p < 0.05$ compared with the IRI+IGF-1C group. Data are presented as $M \pm SD$; $n = 5$. IRI, ischemia–reperfusion injury; IGF-1C, C domain of insulin-like growth factor-1; NP-IGF-1C, nanoparticles of NP-IGF-1C. IL-6, interleukin-6; IL-10, interleukin-10.

In the course of IRI, various forms of cell death, such as necrosis, apoptosis, pyroptosis and ferroptosis, occur. Among these forms, apoptosis is a typical mechanism of renal cell death. When IRI occurs, DNA cleavage and nuclear condensation are observed as the initial indicators of apoptosis [16], and apoptotic cells appear in the proximal, distal and loop areas of renal tubules in the cortex and medulla [17]. The Bcl-2 gene family regulates the progression of AKI by inducing endogenous apoptosis.

When cells suffer from acute injury, proapoptotic factors, including Bax, translocate to the mitochondrial outer membrane, resulting in a significant increase in mitochondrial outer membrane permeabilization (MOMP) and accelerating the apoptotic process [18,19]. Consequently, Bax is used as a primary index to evaluate renal tubular epithelial cell apoptosis [20,21]. As an antiapoptotic protein, Bcl-2 inhibits cell apoptosis, in contrast to Bax, which promotes apoptosis [22]. The detection of apoptosis in

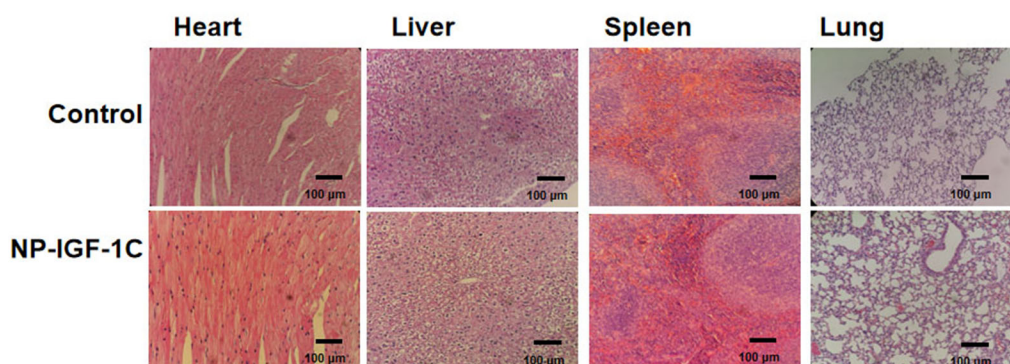


Figure 9. Hematoxylin and eosin (HE) staining of the heart, liver, spleen and lung from the control group and NP-IGF-1C group. Scale bar = 100 µm.

this study showed that NP-IGF-1C exerted an antiapoptotic effect by suppressing Bax expression and increasing Bcl-2 expression.

In the IRI model, IGF-1R expression was upregulated in proximal tubular cells on the third day after injury, indicating that IGF-1 was involved in renal self-repair [23]. In addition, viable renal tubular epithelial cells are the main cell source involved in the process of renal repair and have a strong proliferation ability to replace cells lost due to injury [24]. In contrast, cells that have not undergone regeneration do not express IGF-1 [25]. Thus, the transient expression of IGF-1 during proximal tubule regeneration provides a theoretical foundation for treatment involving recombinant IGF-1. In an experimental model of AKI, IGF-1 treatment increased the glomerular filtration rate through a direct effect on the glomerular vascular system, reduced the resistance of afferent and efferent arteries through the local production of nitric oxide and vasodilatory prostaglandins, and accelerated the recovery of normal renal function and the regeneration of damaged proximal renal tubular epithelial cells [26]. The C domain peptide of insulin-like growth factor-1 (IGF-1), which is composed of 12 amino acids (GYGSSRRAPQT), is considered the active region of IGF-1. By increasing the survival rate of human embryonic stem cells, angiogenesis, and left ventricular wall thickness and reducing adverse cardiac remodeling, IGF-1C promotes the recovery of cardiac function of the ischemic myocardium in mice [27,28].

The stability of commonly used drugs is poor, whereas nanoparticles exhibit good stability and biocompatibility and exert favorable effects on renal therapy. In 1984, a pioneering study by Nefzger et al. [29] was the first to show that polymerized nanoparticles constructed from polymethylmethacrylate penetrate renal tissue from the systemic circulation. In 2003, Tsutsumi and colleagues reported a copolymer system for selective renal administration [30].

With advances in nanotechnology, different nanoparticles have been shown to play important roles in the diagnosis, imaging and treatment of kidney disease. In the present study, the fluorescence imaging property of AIE was used to track nanoparticles *in vivo*, revealing the renal targeting of NP-IGF-1C. In subsequent experiments, we confirmed that NP-IGF-1C markedly improved renal function after IRI and provided new insights into ischemic diseases.

Conclusions

In this paper, we synthesized nanoparticles (NP-IGF1C) to show that NP-IGF-1C is biocompatible and functions as an antioxidant compared to IGF-1C. NP-IGF-1C is enriched in the mouse kidney after renal ischemia–reperfusion injury, with no damage to vital organs. In addition, given its excellent ROS scavenging capacity, NP-IGF-1C alleviates oxidative stress, reduces apoptosis, suppresses the inflammatory response, reduces kidney injury and accelerates renal repair. Compared with conventional medicines, nanomedicines allow poorly soluble drugs to be easily dissolved and absorbed, thus reducing the dose of drug used, enhancing the enrichment at the target site and further enhancing the pharmacological effect. Consequently, NP-IGF-1C may represent a promising drug for ameliorating ischemia–reperfusion injury in the mouse kidney, but additional molecular studies are needed.

Acknowledgments

The authors appreciate Professor Ding Dan at the Academy of Life Science of Nankai University for his scientific research platform and technical guidance.

Disclosure statement

The authors have no potential conflicts of interest to declare.

Funding

This work was financially supported by the “National Natural Science Foundation of China”.

References

- [1] Liangos O, Wald R, O’Bell JW, et al. Epidemiology and outcomes of acute renal failure in hospitalized patients: a national survey. *CJASN*. 2006;1(1):43–51.
- [2] Al-Jaghbeer M, Dealmeida D, Bilderback A, et al. Clinical decision support for in-hospital AKI. *JASN*. 2018;29(2):654–660.
- [3] Beker BM, Corleto MG, Fieiras C, et al. Novel acute kidney injury biomarkers: their characteristics, utility and concerns. *Int Urol Nephrol*. 2018;50(4):705–713.
- [4] Hoste EAJ, Kellum JA, Selby NM, et al. Global epidemiology and outcomes of acute kidney injury. *Nat Rev Nephrol*. 2018;14(10):607–625.
- [5] Liu M, Reddy NM, Higbee EM, et al. The Nrf2 triterpenoid activator, CDDO-imidazolide, protects kidneys from ischemia-reperfusion injury in mice. *Kidney Int*. 2014;85(1):134–141.
- [6] Liu P, Feng Y, Dong D, et al. Enhanced renoprotective effect of IGF-1 modified human umbilical cord-derived mesenchymal stem cells on gentamicin-induced acute kidney injury. *Sci Rep*. 2016;6:20287.
- [7] Wasnik S, Tang X, Bi H, et al. IGF-1 deficiency rescue and intracellular calcium blockade improves survival and corresponding mechanisms in a mouse model of acute kidney injury. *Int J Mol Sci*. 2020;21(11):4095.
- [8] Werle M, Bernkop-Schnurch A. Strategies to improve plasma half life time of peptide and protein drugs. *Amino Acids*. 2006;30(4):351–367.
- [9] Jia Z, Wang X, Wei X, et al. Micelle-forming dexamethasone prodrug attenuates nephritis in Lupus-Prone mice without apparent glucocorticoid side effects. *ACS Nano*. 2018;12(8):7663–7681.
- [10] Shu Y, Yang Y, Zhao Y, et al. Melittin inducing the apoptosis of renal tubule epithelial cells through upregulation of bax/bcl-2 expression and activation of TNF- α signaling pathway. *Biomed Res Int*. 2019;2019:9450368.
- [11] Sharfuddin AA, Molitoris BA. Pathophysiology of ischemic acute kidney injury. *Nat Rev Nephrol*. 2011;7(4):189–200.
- [12] Jang HR, Rabb H. The innate immune response in ischemic acute kidney injury. *Clin Immunol*. 2009;130(1):41–50.
- [13] Lazzeri E, Angelotti ML, Peired A, et al. Endocycle-related tubular cell hypertrophy and progenitor proliferation recover renal function after acute kidney injury. *Nat Commun*. 2018;9(1):1344.
- [14] Basile DP, Anderson MD, Sutton TA. Pathophysiology of acute kidney injury. *Compr Physiol*. 2012;2(2):1303–1353.
- [15] Ouyang W, O’Garra A. IL-10 family cytokines IL-10 and IL-22: from basic science to clinical translation. *Immunity*. 2019;50(4):871–891.
- [16] Schumer M, Colombel MC, Sawczuk IS, et al. Morphologic, biochemical, and molecular evidence of apoptosis during the reperfusion phase after brief periods of renal ischemia. *Am J Pathol*. 1992;140(4):831–838.
- [17] Kelly KJ, Plotkin Z, Dagher PC. Guanosine supplementation reduces apoptosis and protects renal function in the setting of ischemic injury. *J Clin Invest*. 2001;108(9):1291–1298.
- [18] Wolfs TG, de Vries B, Walter SJ, et al. Apoptotic cell death is initiated during normothermic ischemia in human kidneys. *Am J Transplant*. 2005;5(1):68–75.
- [19] Mikhailov V, Mikhailova M, Degenhardt K, et al. Association of bax and bak homo-oligomers in mitochondria. Bax requirement for bak reorganization and cytochrome c release. *J Biol Chem*. 2003;278(7):5367–5376.
- [20] Song H, Han IY, Kim Y, et al. The NADPH oxidase inhibitor DPI can abolish hypoxia-induced apoptosis of human kidney proximal tubular epithelial cells through Bcl2 up-regulation via ERK activation without ROS reduction. *Life Sci*. 2015;126:69–75.
- [21] He P, Zhou G, Qu D, et al. HBx inhibits proliferation and induces apoptosis via fas/FasL upregulation in rat renal tubular epithelial cells. *J Nephrol*. 2013;26(6):1033–1041.
- [22] Huang H, Yu H, Lin L, et al. Protective effect of sonic hedgehog against oxidized lowdensity lipoprotein-induced endothelial apoptosis: Involvement of NF κ B and Bcl2 signaling. *Int J Mol Med*. 2020;45(6):1864–1874.
- [23] Albiston AL, Herington AC. Tissue distribution and regulation of insulin-like growth factor (IGF)-binding protein-3 messenger ribonucleic acid (mRNA) in the rat: comparison with IGF-I mRNA expression. *Endocrinology*. 1992;130(1):497–502.
- [24] Humphreys BD, Valerius MT, Kobayashi A, et al. Intrinsic epithelial cells repair the kidney after injury. *Cell Stem Cell*. 2008;2(3):284–291.
- [25] Andersson G, Jennische E. IGF-I immunoreactivity is expressed by regenerating renal tubular cells after ischaemic injury in the rat. *Acta Physiol Scand*. 1988;132(4):453–457.
- [26] Imberti B, Morigi M, Tomasoni S, et al. Insulin-like growth factor-1 sustains stem cell mediated renal repair. *J Am Soc Nephrol*. 2007;18(11):2921–2928.
- [27] Shafiq M, Zhang Y, Zhu D, et al. In situ cardiac regeneration by using neuropeptide substance P and IGF-1C peptide eluting heart patches. *Regen Biomater*. 2018;5(5):303–316.
- [28] Yao Y, Yang L, Feng LF, et al. IGF-1C domain-modified hydrogel enhanced the efficacy of stem cells in the treatment of AMI. *Stem Cell Res Ther*. 2020;11(1):136.
- [29] Nefzger M, Kreuter J, Voges R, et al. Distribution and elimination of polymethyl methacrylate nanoparticles after peroral administration to rats. *J Pharm Sci*. 1984;73(9):1309–1311.
- [30] Kamada H, Tsutsumi Y, Sato-Kamada K, et al. Synthesis of a poly(vinylpyrrolidone-co-dimethyl maleic anhydride) co-polymer and its application for renal drug targeting. *Nat Biotechnol*. 2003;21(4):399–404.